

# First Experimental Results with the Imaging MIMO Radar MIRA-CLE X

Jens Klare, Olaf Saalman, Helmut Wilden, Andreas R. Brenner

Fraunhofer Institute for High Frequency Physics and Radar Techniques FHR, Wachtberg, Germany  
phone +49 228 9435311, fax +49 228 9435618, e-mail jens.klare@fhr.fraunhofer.de

## Abstract

MIMO radar for imaging is a quite new and promising research field with a big potential for various applications. Three different imaging radars based on the MIMO principle are currently developed at Fraunhofer FHR. This paper describes the ground based X-band MIMO radar MIRA-CLE X. This radar consists of 16 transmit and 14 receive antennas which are arranged in a special way to synthesize a fully and equally spaced virtual antenna array of 224 elements during signal processing. First image results of MIRA-CLE X are presented and discussed.

## 1 Imaging MIMO Radar

Imaging MIMO radar systems using colocated transmit and receive antennas are the keys to various new and promising applications, like environmental monitoring, security surveillance, and assistance systems. For a coherent MIMO radar,  $N_{TX}$  transmit (TX) and  $N_{RX}$  receive (RX) antennas are placed in a particular way (ARTINO<sup>1</sup> principle) in order to form a fully distributed antenna array of  $N_{TX} \times N_{RX}$  virtual elements during signal processing [1] [2]. The virtual antenna elements are located at the centers of gravity between the phase centers of each TX/RX pair (see **Figure 1**).

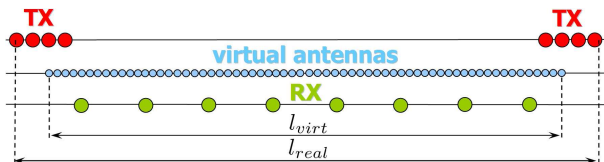


**Figure 1:** Arrangement of TX and RX antennas according to the ARTINO principle.

Three different imaging MIMO radar demonstrators are presently developed at Fraunhofer FHR. The first one is the airborne radar ARTINO which consists of a small UAV with an integrated MIMO antenna in the wings operating in Ka-band. It allows to image the directly overflowed scene in three dimensions [3]. The second radar demonstrator is the ground based Ka-band MIMO radar MIRA-CLE<sup>2</sup> which generates in the basic configuration 256 virtual antenna elements [4]. A main feature of this system is the potential to use waveform- and frequency diversity to increase the SNR and to allow a high PRF [5]. A reasonably high PRF is necessary for instance to image non stationary objects. The third MIMO radar is the X-band system MIRA-CLE X which is presented in this paper.

<sup>1</sup>Airborne Radar for Three-dimensional Imaging and Nadir Observation

<sup>2</sup>MIMO Radar Configurable

## 2 System Specifications

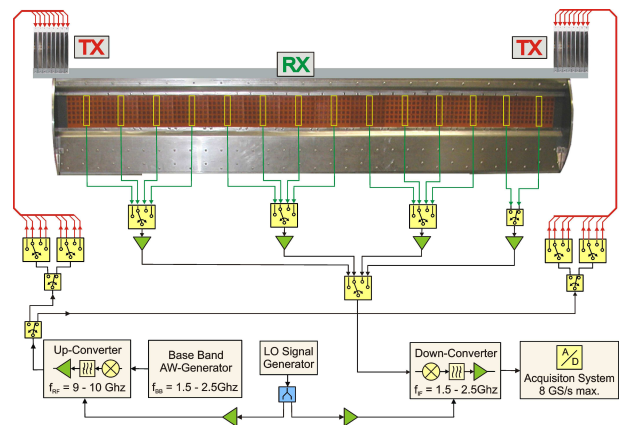


**Figure 2:** MIRA-CLE X: Superposition of the antenna image with the schematic diagram. In the shown MIMO configuration, only a sparse set of patch antennas of the receive antenna is used.

The idea of MIRA-CLE X was to develop a quite cost-efficient X-band MIMO radar made of already available components. The array antenna of MIRA-CLE X has a length of about 2 m (see **Figure 2**). The experimental setup consists of the switching matrix, the signal generation, and the receiver followed by an acquisition unit. The system works at a center frequency of 9.45 GHz and has an instantaneous bandwidth of 1 GHz. The base band signal is generated by an arbitrary waveform generator, mixed upwards to X-band, and amplified. The radiated pulse power amounts to 33 dBm. The expandable and reconfigurable construction allows easily to use more powerful amplifiers for long distance applications. A switching matrix consisting of fast pin diode switches operates the sequential distribution of the transmit and receive power, controlled by a 48-channel pattern generator. The data acquisition is

performed by a fast 8 GS/s sample and recording system. The system RF-paths are constructed with low dispersive components to accomplish the lowest possible group delay variation and gain ripple over the system bandwidth. The system transfer function and all TX/RX path delays have been measured and collected in a calibration matrix to compute an optimal matched filter for an accurate range pulse compression.

The transmit array consists of 16 sector horn antennas which are arranged in two blocks of eight elements at both sides of the receive antenna. The horizontal element spacing is  $0.57\lambda$ . The beamwidth of a single transmit element amounts to  $20^\circ$  in elevation and  $96^\circ$  in azimuth with a gain of 11 dB.

For the receive antenna, only each eighth element of the already existing fully distributed antenna array with 112 elements and an element spacing equal to those of the transmit antenna elements is used. Each element consists of 6 combined and vertically arranged aperture coupled patch radiators. This results in a sparse arrangement of 14 receive elements which are connected to a receive switching matrix. Each receive column has an elevation beamwidth of  $21^\circ$  and an azimuth beamwidth of  $90^\circ$  with a receive antenna gain of 10.5 dB.

In order to form an optimum MIMO arrangement for imaging with equally spaced virtual phase centers, the transmit antenna blocks are located with a horizontal spacing of  $0.285\lambda$  next to the outer receive elements. The transmit and receive arrays are vertically shifted in order to allow a proper assembling. To sum up, 16 transmit and 14 receive elements form a fully and regularly distributed virtual antenna array of 224 virtual elements.

The range dependent spatial resolution in cross-range (**Table 1**) results from the angular resolution of the whole virtual antenna array [3]:

$$\delta y \approx R \frac{\lambda}{2l_{virt}} \quad (1)$$

$l_{virt}$  is the length of the virtual antenna array (see **Figure 1**).

Distance [m]	Azimuth Resolution [m]
50	0.39
100	0.78
200	1.57
400	3.13
600	4.70

**Table 1:** Range dependent azimuth resolution

### 3 Signal-to-Noise Ratio (SNR)

#### 3.1 Before cross-range focusing

The SNR for a single TX/RX antenna pair at a range  $R$  can be expressed after range compression by

$$SNR_1 = \frac{P_{TX}G_{TX}G_{RX}\lambda^2\tau\kappa}{(4\pi)^3R^4JN_f}\sigma_0A_1. \quad (2)$$

$P_{TX}$  denotes the transmit power,  $G_{TX}$  the transmit gain,  $G_{RX}$  the receive gain,  $\lambda$  the radar wavelength,  $\tau$  the pulse length,  $\kappa$  the system losses, the constant  $J = 4 \cdot 10^{-21}$  Ws, and  $N_f$  the noise figure.  $\sigma_0$  is the clutter reflectivity and  $A_1$  the surface of an illuminated resolution cell on the ground. This surface (here at broadside) can be written as the product of the range resolution on the ground  $\Delta R = \frac{c}{2B}$  with the cross-range extend determined by the 3 dB antenna beamwidth  $\Delta\theta$  of a single antenna element

$$A_1 = \frac{c}{2B} \cdot 2R \tan\left(\frac{\Delta\theta}{2}\right). \quad (3)$$

This leads to the SNR

$$SNR_1 = \frac{P_{TX}G_{TX}G_{RX}\lambda^2\tau\kappa \tan\left(\frac{\Delta\theta}{2}\right)c}{B(4\pi)^3R^3JN_f}\sigma_0. \quad (4)$$

#### 3.2 After cross-range focusing

After focusing in cross-range, the surface of a resolution cell on the ground is much narrower and given by

$$A_2 = \frac{c}{2B} \cdot R \frac{\lambda}{2l_{virt}} \quad (5)$$

with  $l_{virt}$  the length of the virtual antenna array. The SNR is therefore changed to

$$SNR_2 = \frac{N_{TX}^2N_{RX}^2P_{TX}G_{TX}G_{RX}\lambda^3\tau\kappa c}{4Bl_{virt}(4\pi)^3R^3JN_f}\sigma_0. \quad (6)$$

The square of the antenna numbers can be explained by the fact that  $N_{TX}N_{RX}$  signals are coherently combined. In addition, the antenna gain is improved by a factor  $N_{TX}N_{RX}$ .

If  $K$  cycles are coherently added, the SNR is improved to  $SNR_3 = K SNR_2$ .

## 4 Experimental Setup and Results

### 4.1 System Setup

Time multiplexing was used in order to get all TX/RX combinations. For this, one TX antenna was activated for  $N_{RX}$  pulses and the receiver was switched successively from one RX antenna to the other from pulse to pulse. This switching schema was repeated with all transmit antennas (called a 'cycle') resulting in 224 combinations. Several

cycles were conducted consecutively in order to increase the SNR during signal processing by coherent integration after range compression. For the first trial, a scene in the rhine valley at Bonn-Mehlem was chosen (see **Figures 3** and **4**). This area contains both urban and rural areas. The radar was placed on top of a small hill at a height about of 146 m (see **Figure 5**).



**Figure 3:** Radar view from a small hill.



**Figure 4:** Orthophoto of the imaged scene. © Landesvermessungsamt NRW.



**Figure 5:** MIRA-CLE X Antenna

The lowest part of the imaged scene has a height of about 60 m. The pulse length of  $0.5 \mu s$  allowed to image also the nearest objects in the scene. The system settings are shown in **Table 2**.

Pulse length	$0.5 \mu s$
Receive window length	$4.1 \mu s$
Slant range	615 m
Sampling rate	8 GS/s
Depression angle	$15^\circ$

**Table 2:** System settings

## 4.2 Image reconstruction

In a first step, the radar data were range compressed for each virtual antenna. Afterwards, the range compressed data were Hilbert transformed and down converted to base-band. A Hamming window was applied to reduce the side lobes. Since each TX and each RX channel suffers from different small delays (e. g. due to different cable lengths), a time shift correction was applied. Then, the data from several cycles were coherently summed up to increase the SNR. For the presented experiment, 24 cycles were used resulting in a gain of 13.8 dB. **Figure 6** shows the resulting range profiles for the different virtual antennas.

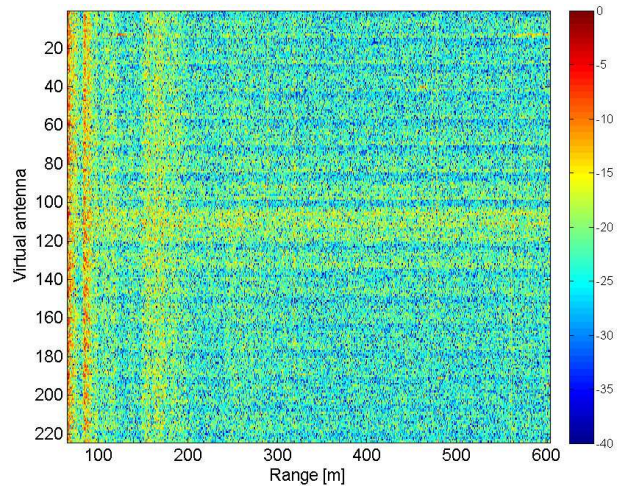


**Figure 6:** Range compressed data for each virtual antenna.

After pre-processing, two different processing approaches were used for focusing in cross-range. The first approach uses a beam forming operation for each range/angle cell to sum up the contributions for each virtual antenna after phase correction (see **Figure 7**). These data were transformed afterwards to a Cartesian grid shown in **Figure 8**. This transformation is, however, quite time consuming. The beam forming operation becomes more time consuming under near field conditions since a selective beam-forming operation [6] has to be applied. In the second approach, a back projection algorithm was used (see **Figure 9**). Since the data are directly back projected to a Cartesian

coordinate grid, no near field case has to be assumed. The calculations are very time consuming.

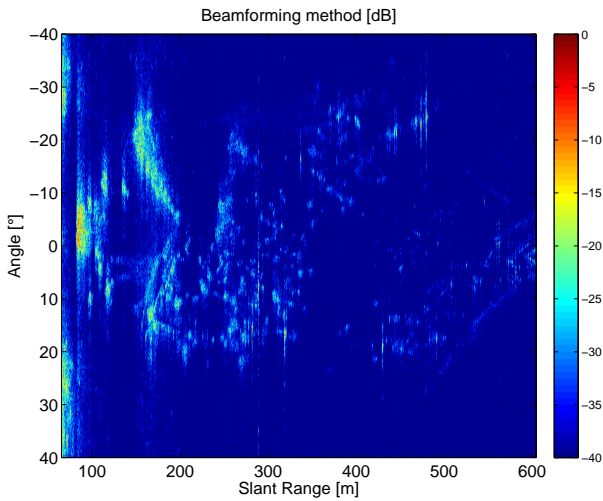


**Figure 7:** Radar image (beamforming method).

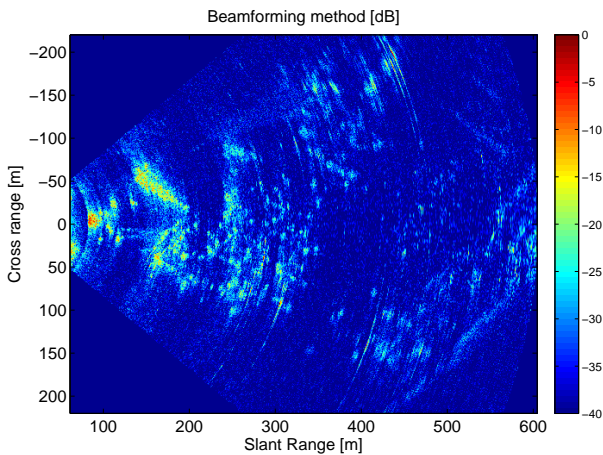


**Figure 8:** Radar image after transformation to a Cartesian grid (beamforming method).

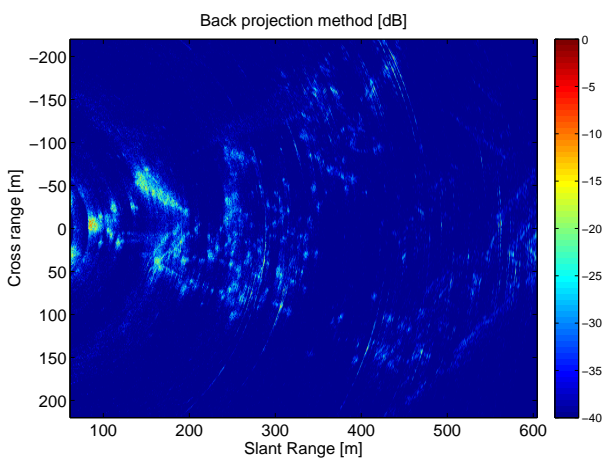


**Figure 9:** Radar image (back projection method).

### 4.3 Discussion

A comparison of the radar image with the photo from the viewpoint of the radar and with the ortho photo shows a very well agreement. Right in front of the radar at about 80 m were some trees which are clearly visible and distinguishable in the radar image ('A' in the ortho photo). Between 150 m and 200 m at  $\varphi = -5^\circ \dots -25^\circ$  or for a cross-range between -10 m and -70 m is a dominant row of trees visible ('B' in the ortho photo). A tall building ('C' in the ortho photo) produces strong scatterers in the radar image at  $R \approx 430$  m. The farthest structure in the radar image is a long tree row for a range between 450 m and 600 m ('D' in the ortho photo). One has to note, that a part of the village (for a range between 300 m and 400 m) was in the radar shadow.

The SNR difference between the mean SNR of figure 6 and figure 9 is 20.5 dB. According to equations 4 and 6 the ratio between the two SNRs is given by  $\frac{N_{TX}^2 N_{RX}^2 \lambda}{4L_{virt} \tan(\frac{\Delta\theta}{2})}$ . This yields with the MIRA-CLE X's parameters to 19.8 dB, which is in a good agreement to the measured value.

The MIMO principle for radar imaging was successfully demonstrated with the radar demonstrator MIRA-CLE X.

### References

- [1] J. H. G. Ender and J. Klare, "System architectures and algorithms for radar imaging by MIMO-SAR," in *IEEE RadarCon 2009*, Pasadena, USA, May 2009, pp. 1–6.
- [2] J. Li, P. Stoica, and X. Zheng, "Signal synthesis and receiver design for MIMO radar imaging," *Signal Processing, IEEE Transactions on*, vol. 56, no. 8, pp. 3959–3968, Aug. 2008.
- [3] J. Klare, A. R. Brenner, and J. H. G. Ender, "A new airborne radar for 3D imaging - image formation using the ARTINO principle," in *Proc. EUSAR 2006*, Dresden, Germany, May 2006, p. ID 103.
- [4] H. Wilden, J. Klare, A. Fröhlich, and M. Krist, "MIRA-CLE, an experimental MIMO radar in Ka-band," in *EUSAR 2010*, Aachen, Germany, June 2010.
- [5] J. Klare, "Digital beamforming for a 3D MIMO SAR - improvements through frequency and waveform diversity," in *Proc. IEEE International Geoscience and Remote Sensing Symposium IGARSS 2008*, vol. 5, Boston, USA, July 2008, pp. V 17–20.
- [6] J. Klare, A. R. Brenner, and J. H. G. Ender, "Impact of platform attitude disturbances on the 3D imaging quality of the UAV ARTINO," in *Proc. EUSAR 2008*, vol. 4, Friedrichshafen, Germany, June 2008, pp. 191–194.